research papers

X-ray diffraction and Raman study of DL-alanine at high pressure: revision of phase transitions

Nikolay A. Tumanov[a,b]* and Elena V. Boldyreva[a,b]*

[a]Institute of Solid State Chemistry and Mechanochemistry SB RAS, Kutateladze 18, Novosibirsk 630128, Russian Federation, and [b]REC-008, Novosibirsk State University, Pirogova 2, Novosibirsk 630090, Russian Federation

Correspondence e-mail:
n.tumanov@gmail.com,
eboldyreva@yahoo.com

The effect of pressure on DL-alanine has been studied by X-ray powder diffraction (up to 8.3 GPa), single-crystal X-ray diffraction and Raman spectroscopy (up to $\sim$ 6 GPa). No structural phase transitions have been observed. At $\sim$ 1.5–2 GPa, cell parameters b and c become accidentally equal to each other, but the space-group symmetry does not change. There is no phase transition between 1.7 and 2.3 GPa, contrary to what has been reported earlier [Belo *et al.* (2010). *Vibr. Spectrosc.* **54**, 107–111]. The presence of the second phase transition, which was claimed to appear within the pressure range from 6.0 to 7.3 GPa (Belo *et al.*, 2010), is also argued. The changes in the Raman spectra have been shown to be continuous in all the pressure ranges studied.

1. Introduction

The polymorphism of amino acids attracts much attention because of their importance as materials, drugs and biomimetics (Boldyreva, 2007, 2008*a*,*b*, 2009; Moggach *et al.*, 2008; Freire, 2010). Most publications deal with L-forms of amino acids, since they are involved in various biological processes. However, there is a number of papers in which the behavior of L- and DL-forms of several amino acids was compared by analyzing calorimetric, diffraction and spectroscopic data at variable conditions. As far as variable pressures are concerned, to the best of our knowledge, chiral and racemic counterparts have been compared for serine (Kolesnik *et al.*, 2005; Moggach *et al.*, 2005, 2006; Boldyreva, Sowa *et al.*, 2006) and cysteine (Moggach, Allan *et al.*, 2006; Minkov *et al.*, 2008; Minkov, Goryainov *et al.*, 2010; Minkov, Tumanov *et al.*, 2010) only. Interestingly, the behavior of L- and DL-forms of these amino acids upon varying pressure is significantly different. Thus, two first-order phase transitions caused by a discontinuous change in the orientation of the OH group and a corresponding rearrangement in the hydrogen-bond network were revealed for L-serine at pressures of 4.0–5.4 and 7.8 GPa, respectively (Kolesnik *et al.*, 2005; Moggach *et al.*, 2005, 2006; Boldyreva, Sowa *et al.*, 2006; Drebushchak *et al.*, 2006), whereas the changes in the structure of DL-serine are continuous up to 8.6 GPa (Kolesnik *et al.*, 2005; Boldyreva, Kolesnik *et al.*, 2006). Another behavior has been observed for chiral and racemic counterparts of cysteine. At ambient conditions, L-cysteine has orthorhombic [L-cysteine-(I)] and monoclinic [L-cysteine-(II)] polymorphs. Upon increasing the pressure, phase transitions were found for both of them. In L-cysteine-(I) a series of phase transitions occurs in the pressure range of 1.1–3 GPa; these phase transitions led to the formation of L-cysteine-(III) (Moggach, Allan *et al.*, 2006; Minkov *et al.*, 2008; Minkov, Goryainov *et al.*, 2010). The phase transitions proceed with hysteresis and cause the formation of several inter-

mediate phases, among which only the structure of L-cysteine-(IV) was solved (Moggach, Allan *et al.*, 2006). In the structure of L-cysteine-(II) two reversible phase transitions were revealed at ~ 2.9 and ~ 3.9 GPa from Raman spectroscopy data (Minkov, Goryainov *et al.*, 2010). DL-Cysteine also undergoes several phase transitions under pressure; and the first phase transition causing the formation of DL-cysteine-(II) [previously observed at low temperature (Minkov *et al.*, 2009)] occurs at a relatively low pressure of around 0.1 GPa (Minkov *et al.*, 2008; Minkov, Tumanov *et al.*, 2010).

It is important to note that in the studied pairs of L-/DL-amino acids the side chain ($R = -CH_2-SH$ in cysteine and $R = -CH_2-OH$ in serine) is involved in the formation of the hydrogen-bond network in the crystal, and a phase transition leads to a significant change in its orientation and contacts. In this context it was interesting to compare the behavior of structures for which the side chain cannot significantly alter its orientation and does not take part in hydrogen bonding. Hence, alanine $NH_3^+(CHCH_3)COO^-$ ($R = -CH_3$) was selected as the most suitable system.

The behavior of L-alanine has been thoroughly studied earlier by different methods. It has been recently shown that the ambient-pressure crystalline phase of L-alanine is preserved up to 13.6 GPa (Funnell *et al.*, 2010, 2011; Tumanov *et al.*, 2010) and that no phase transitions from the ortho-rhombic into the tetragonal phase and then into the mono-clinic phase, which were reported earlier (Teixeira *et al.*, 2000; Staun Olsen *et al.*, 2006, 2008), in fact occur. Despite the difference in space-group symmetry ($P2_12_12_1$ and $Pna2_1$, respectively), a close relationship between the structures of L- and DL-alanine has been outlined by Simpson & Marsh (1966), and more recently reported in detail (Destro *et al.*, 2008). These structures have similar unit-cell parameters and hydrogen-bond networks. Moreover, the structure of L-alanine can be derived from that of DL-alanine by reflecting the columns of D-molecules with respect to an (001) plane and translating them along the *c* axis, until the proper formation of N—H···O hydrogen bonds becomes possible. Taking into account this similarity, we expected similar behavior for the structures of L- and DL-alanine under high pressure. Recently, three phase transitions in the structure of DL-alanine at high pressure (between 1.7 and 2.3 GPa, 6.0 and 7.3 GPa, 11.6 and 13.2 GPa) were inferred by Belo *et al.* (2010) from Raman spectroscopic data. Two of these phase transitions were claimed to occur within the same pressure range as reported initially for L-alanine (Teixeira *et al.*, 2000; Staun Olsen *et al.*, 2006, 2008), results that could not be confirmed by later investigations (Tumanov *et al.*, 2010; Funnell *et al.*, 2010, 2011). By that time we already had X-ray powder diffraction data for DL-alanine, according to which no phase transitions occurred at least up to 8.3 GPa. Due to this discrepancy between our powder diffraction data and the results reported by Belo *et al.* (2010), we decided to analyze the structure of DL-alanine in more detail. For this purpose, we used single-crystal X-ray diffraction and Raman spectroscopy under the same condi-tions on the same single crystal in order to make a comparison between the results from the two methods as reliable as

possible. For high-pressure research this is especially impor-tant: if Raman and X-ray diffraction experiments are run for different samples independently, a correlation of results may not be straightforward because:

(i) the exact pressure values in the cell may be not the same in the two series of experiments, and

(ii) the results may be strongly dependent on kinetic factors (Boldyreva, 2007).

Thus, the aim of the present study was to revise the exis-tence of pressure-induced phase transitions in crystalline DL-alanine by powder and single-crystal X-ray diffraction and Raman spectroscopy, and to compare the structural responses of L- and DL-alanine to increasing pressure.

2. Experimental

DL-Alanine was purchased from ICN Biomedicals (Aurora, Ohio, USA). Small crystals of good quality for single-crystal experiments were selected from the batch; for experiments with powders, the sample was gently ground. Hydrostatic pressure in the powder diffraction experiments was created in a modified Merrill–Bassett diamond anvil cell (DAC) without Be supports (Ahsbahs, 2004; Sowa & Ahsbahs, 2006; a gasket material is Thyrodur-2709, a starting thickness of 0.180 mm, pre-indented to 0.104 mm and then hardened by heating at 773 K for 6 h in micronized iron oxide and by subsequent cooling, a hole diameter of 0.3 mm; Ahsbahs, 1996). Boehler–Almax DACs (Boehler, 2006) were used in single-crystal diffraction and Raman spectroscopy experiments (a stainless steel gasket, a starting thickness of 0.200 mm, pre-indented to 0.120 mm, a hole diameter of 0.3 mm). In all the experiments, pressure was estimated from a shift in the R_1 band of a ruby calibrant ($\pm$ 0.05 GPa; Forman *et al.*, 1972; Piermarini *et al.*, 1975). A methanol:ethanol (4:1) mixture [a (quasi)hydrostatic limit of 10.4 GPa; Piermarini, 1973] was used as a pressure-transmitting liquid in all the experiments.

High-resolution X-ray powder diffraction experiments were carried out using a synchrotron radiation source (λ = 0.7014 Å, a MAR345 two-dimensional image-plate detector) at the BM1A station at the Swiss–Norwegian Beamline at ESRF in Grenoble. The frames were measured at 13 pressure points up to 8.3 GPa with an exposure time of 600 s. The sample-to-detector distance was ~ 340 mm. Silicon powder was used for the calibration of the sample-to-detector distance.

Single-crystal X-ray diffraction experiments were carried out using an Oxford Diffraction Xcalibur Gemini Ultra R diffractometer (Mo $K\alpha$ radiation, 0.5 mm collimator, graphite monochromator, ω-scan, scan step of 0.5°, 40–60 s per frame); the measurements were made at 13 pressure points up to 6.0 GPa. X-ray data were collected every 0.5 GPa and Raman spectra from the same crystal in the same DAC were measured approximately every 0.25 GPa. Collection of the X-ray data was performed using *CrysAlis Pro* software (Oxford Diffrac-tion, 2010). We used the strategy described in Budzianowski & Katrusiak (2004), but in a slightly modified form in order to avoid goniometer collision of our instrument. The same

Table 1
Experimental details (single-crystal diffraction).

For all structures: $C_3H_7NO_2$, M_r = 89.10, orthorhombic, $Pna2_1$, Z = 4. Experiments were carried out at 293 K with Mo $K\alpha$ radiation using an Oxford Diffraction Gemini Ultra R diffractometer. Absorption in a diamond–anvil cell was corrected analytically using *Absorb*6.1 (Angel, 2004). Refinement was on 57 parameters with 1 restraint. H-atom parameters were constrained.

	0.1 GPa	0.5 GPa	1.0 GPa	1.5 GPa	2.0 GPa
Crystal data					
a, b, c (Å)	11.994 (2), 6.0103 (16), 5.8421 (5)	11.938 (3), 5.9485 (18), 5.8266 (6)	11.852 (2), 5.8715 (14), 5.8057 (5)	11.7991 (15), 5.7917 (15), 5.7900 (4)	11.770 (3), 5.751 (4), 5.7748 (8)
V (Å^3)	421.13 (15)	413.75 (16)	404.02 (12)	395.67 (12)	390.9 (3)
μ (mm^{-1})	0.12	0.12	0.12	0.13	0.13
Crystal size (mm)	0.16 × 0.10 × 0.06	0.16 × 0.10 × 0.06	0.16 × 0.10 × 0.06	0.16 × 0.10 × 0.06	0.16 × 0.10 × 0.06
Data collection					
T_{min}, T_{max}	0.399, 0.478	0.397, 0.478	0.406, 0.478	0.417, 0.476	0.410, 0.478
No. of measured, independent and observed [$I > 2\sigma(I)$] reflections	3719, 647, 487	3677, 640, 502	3497, 607, 472	2319, 462, 385	3228, 564, 432
R_{int}	0.068	0.062	0.060	0.056	0.079
$(\sin\theta/\lambda)_{max}$ (Å^{-1})	0.727	0.723	0.724	0.635	0.726
Refinement					
$R[F^2 > 2\sigma(F^2)]$, $wR(F^2)$, S	0.040, 0.077, 1.03	0.042, 0.081, 1.05	0.039, 0.069, 1.02	0.037, 0.067, 1.05	0.046, 0.081, 1.06
No. of reflections	647	640	607	462	564
$\Delta\rho_{max}$, $\Delta\rho_{min}$ (e Å^{-3})	0.11, −0.11	0.14, −0.13	0.14, −0.14	0.13, −0.14	0.13, −0.15

	2.5 GPa	3.0 GPa	3.6 GPa	4.1 GPa	4.5 GPa
Crystal data					
a, b, c (Å)	11.677 (2), 5.705 (2), 5.7311 (8)	11.6535 (18), 5.681 (3), 5.7217 (6)	11.617 (3), 5.611 (4), 5.7156 (15)	11.5877 (17), 5.617 (3), 5.6894 (5)	11.572 (4), 5.567 (5), 5.6710 (11)
V (Å^3)	381.76 (18)	378.8 (2)	372.6 (3)	370.3 (2)	365.4 (3)
μ (mm^{-1})	0.13	0.13	0.13	0.13	0.14
Crystal size (mm)	0.16 × 0.10 × 0.06	0.16 × 0.10 × 0.06	0.16 × 0.10 × 0.06	0.16 × 0.10 × 0.06	0.16 × 0.10 × 0.06
Data collection					
T_{min}, T_{max}	0.406, 0.478	0.408, 0.478	0.410, 0.477	0.407, 0.478	0.408, 0.478
No. of measured, independent and observed [$I > 2\sigma(I)$] reflections	2540, 571, 428	3073, 510, 399	1714, 477, 359	3067, 528, 420	2420, 529, 385
R_{int}	0.063	0.070	0.062	0.064	0.078
$(\sin\theta/\lambda)_{max}$ (Å^{-1})	0.730	0.725	0.719	0.728	0.725
Refinement					
$R[F^2 > 2\sigma(F^2)]$, $wR(F^2)$, S	0.042, 0.069, 0.99	0.037, 0.059, 1.00	0.040, 0.073, 1.00	0.040, 0.063, 1.03	0.041, 0.078, 0.95
No. of reflections	571	510	477	528	529
$\Delta\rho_{max}$, $\Delta\rho_{min}$ (e Å^{-3})	0.14, −0.15	0.13, −0.14	0.15, −0.15	0.14, −0.12	0.15, −0.14

	5.0 GPa	5.5 GPa	6.0 GPa
Crystal data			
a, b, c (Å)	11.537 (3), 5.554 (3), 5.6456 (8)	11.4915 (17), 5.5249 (18), 5.6262 (5)	11.452 (3), 5.516 (3), 5.6060 (7)
V (Å^3)	361.7 (2)	357.21 (13)	354.10 (19)
μ (mm^{-1})	0.14	0.14	0.14
Crystal size (mm)	0.16 × 0.10 × 0.06	0.16 × 0.10 × 0.06	0.16 × 0.10 × 0.06
Data collection			
T_{min}, T_{max}	0.408, 0.478	0.409, 0.478	0.410, 0.478
No. of measured, independent and observed [$I > 2\sigma(I)$] reflections	3018, 499, 396	2999, 512, 425	2988, 511, 387
R_{int}	0.075	0.068	0.072
$(\sin\theta/\lambda)_{max}$ (Å^{-1})	0.726	0.718	0.724
Refinement			
$R[F^2 > 2\sigma(F^2)]$, $wR(F^2)$, S	0.042, 0.079, 1.05	0.041, 0.071, 1.09	0.040, 0.071, 1.00
No. of reflections	499	512	511
$\Delta\rho_{max}$, $\Delta\rho_{min}$ (e Å^{-3})	0.16, −0.15	0.15, −0.13	0.14, −0.13

Computer programs used: *CrysAlis Pro* (Oxford Diffraction Ltd, 2010), *SHELXS*97, *SHELXL*97 (Sheldrick, 2008), *Mercury* (Macrae *et al.*, 2008), *PLATON* (Spek, 2009), *enCIFer* (Allen *et al.*, 2004).

Table 2
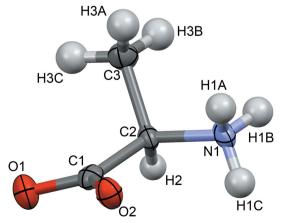Unit-cell parameters (Å, °) and volume from powder diffraction data.

No.	Pressure (GPa)	a (Å)	b (Å)	c (Å)	Volume (Å³)
1	0†	12.017 (4)	6.034 (3)	5.828 (2)	422.6 (2)
2	0.4	11.978 (7)	5.957 (4)	5.844 (3)	417.0 (3)
3	0.6	11.872 (4)	5.884 (3)	5.803 (2)	405.3 (2)
4	1.3	11.784 (6)	5.801 (3)	5.777 (3)	394.9 (3)
5	1.4†	11.801 (4)	5.812 (3)	5.786 (2)	396.8 (2)
6	1.7	11.728 (2)	5.766 (3)	5.758 (3)	389.3 (2)
7	2.7	11.631 (4)	5.687 (3)	5.715 (1)	378.1 (2)
8	3.4	11.583 (7)	5.642 (4)	5.691 (2)	371.9 (2)
9	4.3	11.519 (5)	5.585 (3)	5.659 (3)	364.0 (2)
10	5.4	11.457 (3)	5.538 (2)	5.616 (1)	356.3 (1)
11	6.3	11.409 (4)	5.490 (4)	5.581 (3)	349.5 (2)
12	7.5	11.364 (3)	5.447 (1)	5.540 (1)	343.0 (1)
13	8.3	11.321 (7)	5.418 (3)	5.511 (3)	338.0 (2)

† Diffraction patterns are measured on decompression.

strategy was used for all single-crystal experiments, only the time per frame was sometimes varied. The completeness of the datasets was 43–55% depending on the experiment. The initial dimensions of the crystals were $0.16 \times 0.10 \times 0.06$ mm.

Raw powder diffraction data were processed (calibration, masking of the reflections from diamond and ruby, integration) using the *Fit*2D program (Hammersley *et al.*, 1996). The powder patterns were indexed using *DICVOL*06 (Boultif & Louër, 2004) and *WinXPOW* (Stoe & Cie, 2007) software. The search for indexing solutions was carried out among all crystal systems except the triclinic one.

Single-crystal data were reduced using *CrysAlis Pro* software. First, the peak-hunting procedure with preliminary background subtraction was run in order to exclude peaks from the gasket material. After that the unit cell was determined as usual; if the search for a unit cell produced that of the diamond, the corresponding peaks were omitted and the unit cell search was started again. Normally, the unit cell of the sample was found from the first to the third trial. The unit cell was transformed in accordance with the standard settings for the *Pna*2₁ space group, in order to simplify further data reduction. The data were reduced as from a single-crystal

Figure 1
A displacement ellipsoid plot of DL-alanine at 6.0 GPa showing the atom-numbering scheme and 50% probability displacement ellipsoids. H atoms are shown as spheres of arbitrary size.
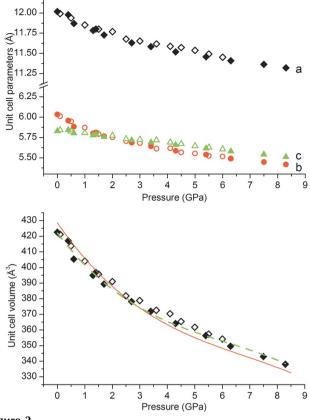

Figure 2
The unit-cell parameters (*a*) and volume (*b*) of DL-alanine *versus* pressure (*a*: black rhombus, *b*: red circles, *c*: green triangles). Open symbols – single-crystal diffraction; filled symbols – powder diffraction. Green dashed line approximates the powder diffraction data for DL-alanine. Red solid line – volume of L-alanine (Tumanov *et al.*, 2010). This figure is in color in the electronic version of the paper.

sample, without taking the reflections from diamond into account. The overlapping of the reflections from the sample and diamond was checked manually afterwards, and the affected reflections were excluded. Absorption by diamonds was corrected numerically using *Absorb*6.1 (Angel, 2004) software. The structures were solved and refined with the standard *SHELX* (Sheldrick, 2008) procedures using the X-Step32 shell (Stoe & Cie, 2002). All non-H atoms were refined in the anisotropic approximation. H atoms were placed geometrically. Experimental details and refinement parameters for single-crystal experiments are given in Table 1. The refined unit-cell parameters from powder experiments are summarized in Table 2. Structural models are given in the CIF in the supplementary material.[1] The molecular geometry and numeration of atoms are shown in Fig. 1. *Mercury* (Macrae *et al.*, 2008) and *PLATON* (Spek, 2009) programs were used for visualization and analysis. Hirshfeld surfaces were calculated using *CrystalExplorer* (McKinnon *et al.*, 2004, 2007; Wolff *et al.*, 2007). Contact-surface voids were calculated using *Mercury CSD 2.3* (Macrae *et al.*, 2008) with a probe radius of
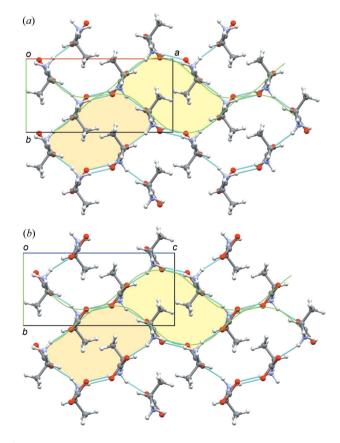
0.2 Å and an approximate grid spacing of 0.1 Å. For a better visual representation of the structural changes the probe radius was set to be 0.5 Å and the grid step was taken to be 0.1 Å (the minimum possible value). At a smaller probe radius visualization was less clear since the voids overlapped with the molecules, and the voids having large radii did not exist in the structure at the highest pressures.

Raman spectra upon increasing the pressure were measured in backscattering geometry using a Horiba Jobin Yvon Lab-Ram HR spectrometer equipped with a N_2-cooled CCD-2048 × 512 detector coupled to an Olympus BX41 microscope. Excitation was supplied by an argon ion laser (λ = 488 nm) with a 4 cm^{-1} spectral resolution.

3. Results and discussion

3.1. X-ray diffraction analysis

Pressure-induced changes in the unit-cell parameters and the volume of DL-alanine, according to X-ray powder and single-crystal diffraction data, are shown in Fig. 2. The changes were continuous; no phase transitions occurred at least up to 8.3 GPa. Modulus of dilation [$\Delta = \epsilon_{ii} = (V_p - V_{amb})/V_{amb}$, where ϵ_{ij} is a component of strain tensor, V_{amb} and V_p represent the unit-cell volume at ambient and high pressure, respectively] of DL-alanine is larger than that of L-alanine at the same pressure. The unit-cell volume of L-alanine at ambient pressure is slightly ($\sim$ 1.5%) larger than that of DL-alanine, but the two volumes become equal to each other at $\sim$ 3 GPa. At 8.3 GPa, the highest pressure achieved in our experiments, the unit-cell volume of L-alanine is noticeably smaller ($\sim$ 1.2%) than the volume of DL-alanine. So, at ambient pressure L- and DL-alanine seem to satisfy Wallach's rule (Wallach, 1895),[2] but above 3 GPa this pair becomes an exception to this rule. Two unit-cell parameters of DL-alanine became equal at a pressure of around 1.5–2.0 GPa, similar to what has been observed previously for L-alanine (Tumanov *et al.*, 2010). This accidental coincidence of the two parameters, however, does not imply the formation of a tetragonal phase, since the symmetry of the structure remains orthorhombic and the values of the cell parameters diverge as pressure is increased further. At the same pressure, the maximum linear strain[3] of DL-alanine was observed along the *b* axis, while the minimum linear strain was along the *a* and *c* axes. This correlates well with the directions of chains formed by hydrogen bonds. A low linear strain along the *c* axis is easily explained by the fact that this particular direction coincides with the direction of 'head-to-tail' chains formed by strong NH···O hydrogen bonds, which are known to be very robust in all the amino-acid crystal structures (Vinogradov, 1979; Görbitz, 1989). The reason for the low linear strain along the *a* axis is less evident, but can be associated with the presence of

zigzag chains formed by molecules linked through strong NH···O hydrogen bonds (Fig. 3). Cyclic motifs, in the center of which there are CH_3 groups of two molecules, can be distinguished in the general three-dimensional hydrogen-bonded network. Under pressure, whole molecules are noticeably shifted along the *b* axis, thereby providing the maximum linear strain along this direction. This shift could be easily noticed by observing the position of CH_3 groups (Fig. 4). In our case, as is typical for molecular crystals, because of the anisotropy of compression, it was not possible to adequately describe the compression of the structure by giving a single value of compressibility, or bulk modulus, or the equation of state parameters. The anisotropy of strain in L-alanine is similar to that in DL-alanine. In order to numerically compare the responses of the structures to pressure, we took the pressure of 8.3 GPa; at this pressure, the unit-cell parameters of both compounds were determined and the values of linear strain in three crystallographic directions were compared. The minimum linear strain observed along 'head-to-tail' chains of alanine zwitterions (*a* axis for L-alanine, *c* axis for DL-alanine) was smaller in L-alanine (−4.8% at 8.3 GPa) compared with DL-alanine (−5.4% at 8.3 GPa). The maximum linear strain,
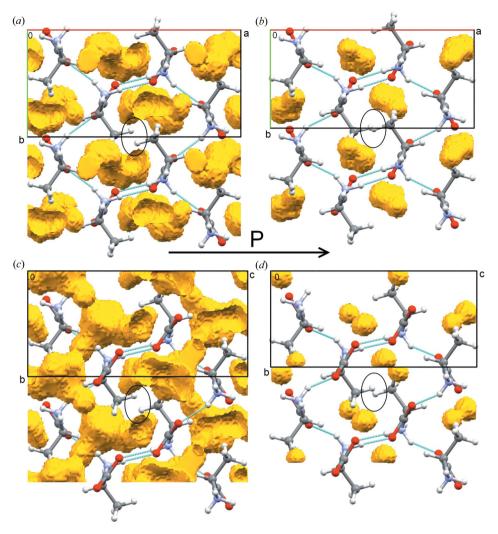

Figure 3
Fragments of (*a*) the DL-alanine structure at 0.1 GPa and (*b*) L-alanine at 0.2 GPa. Head-to-tail chains are normal to the plane. Green lines show the 'wavy' motifs of hydrogen bonds along the *a* axis (DL-alanine) and along the *c* axis (L-alanine). A pale yellow color defines the possible partitioning of the structure into areas, each locating the CH_3 groups inside.

---

[2] For example, this pair of compounds was used as an example in the work of Brock *et al.* (1991) discussing Wallach's rule.
[3] In case of orthorhombic crystal system, principal axes of strain tensor coincide with crystallographic axes, so linear strain ($\epsilon_i = a_{i,p} - a_{i,amb})/a_{i,amb}$, where $a_{i,amb}$ and $a_{i,p}$ are the values of the *i*th unit-cell parameter at ambient and high pressure, respectively.

Figure 4
Visualization of voids in the structures of (*a*), (*b*) DL-alanine and (*c*), (*d*) L-alanine at 0.1 (*a*), (*c*) and 6.0 GPa (*b*), (*d*). Voids were determined using the 'rolling ball' method with probe radius 0.5 Å and grid 0.1 Å. The most significant change in the structure, *i.e.* shift of the molecules along the *b* axis, is shown with ovals.

and valence angles, but with free rotation of NH_3/CH_3 groups along the CN/CC bond, so that the changes in the orientation of these groups *versus* pressure could be analyzed. The torsion angle H1*A*—N1—C2—C1, which characterizes the orientation of the NH_3 group, changed by no more than 2°. This change seems to be within experimental error and not related to the changes in the molecular structure itself. The pressure dependence of the H3*A*—C3—C2—C1 torsion angle, which characterizes the orientation of the CH_3 group, did not show a particular trend either, but the magnitude of the effect was somewhat larger than for the NH_3 group (approximately 5° upon varying pressure from 0.1 to 6.0 GPa); but with the limitations in the quality of data collected at high pressure in a DAC taken into account, this effect is still practically negligible for the molecular geometry.

The changes in carboxylic group are of more interest. In our previous study of L-alanine (Tumanov *et al.*, 2010), two C—O intramolecular bonds in the carboxyl group were shown to become more equivalent with increasing pressure. This phenomenon was supposed to be caused by a shift of the proton within the N—H···O hydrogen bond. This effect was originally overlooked in Funnell *et al.* (2010), since the C—O bonds were assumed to be equal in refinement, but was confirmed in more recent work by the same group (Funnell *et al.*, 2011) on the basis of DFT calculations. In the structure of DL-alanine, however, the difference in C—O bond lengths practically did not change with increasing pressure, at least within experimental error (Fig. 5*a*). The different effect of pressure on the carboxyl groups in L- and DL-alanine can be interpreted in terms of the changes in the NH···O hydrogen bonds. In the structure of L-alanine, a hydrogen bond, which is the longest one at ambient conditions, becomes the shortest one as pressure increases, thereby causing a redistribution of protons in hydrogen bonds surrounding the carboxyl group and, consequently, making the values of the C—O bond lengths closer (Tumanov *et al.*, 2010). In the structure of DL-alanine, however, relative compressions of all the three types of NH···O hydrogen bonds are approximately the same (Fig. 5*b*). As a consequence, the bond, which is the longest one at ambient conditions, remains the

both in L-alanine and in DL-alanine, was observed along the crystallographic *b* axis,[4] but linear strain in this direction was smaller for L-alanine (−11.6% at 8.3 GPa) compared with DL-alanine (−10.2% at 8.3 GPa). Linear strain in the direction of the third principal axis at 8.3 GPa was −7.5% for L-alanine and −5.8% for DL-alanine.
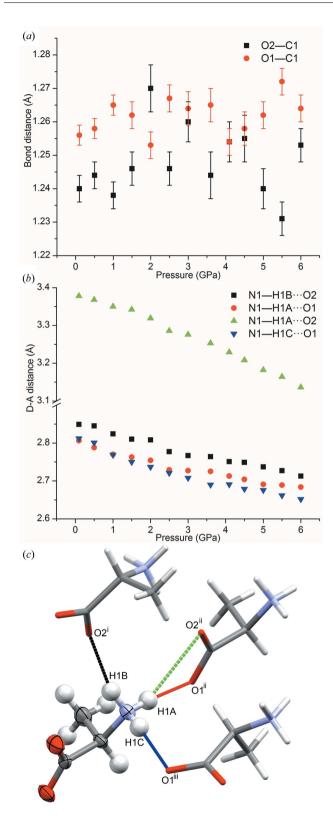
The molecular geometry of alanine changed only slightly with pressure: the most considerable alteration was a smooth rotation of the carboxyl group, during which the value of the O2—C1—C2—N1 torsion angle decreased from 19.1 (4)° at 0.1 GPa to 9.0 (5)° at 6.0 GPa. The positions of H atoms in the NH_3 and CH_3 groups were refined with fixed bond distances

---

[4] Since the choice of notations for the unit-cell parameters in the case of DL-alanine was defined by the standard setting of the space group $Pna2_1$, the notations of the crystallographic axes in L- and DL-alanine corresponding to similar directions in the structures do not coincide. The *a* axis of L-alanine corresponds to the *c* axis of DL-alanine, the *b* axis to the *b* axis and the *c* axis to the *a* axis, respectively.
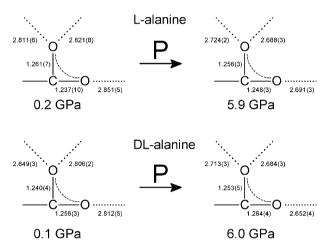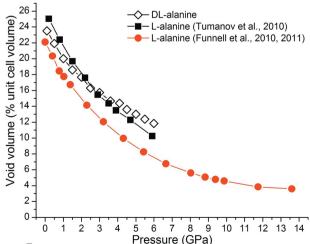
Figure 5
(a) Intramolecular C—O distances and (b) N—O distances in the NH···O hydrogen bonds and a contact, as defined in (c), versus pressure. The colors of lines showing hydrogen bonds in (c) correspond to the colors of symbols at plot (b). This figure is in color in the electronic version of this paper. Symmetry codes: (i) $1 - x, 1 - y, -\frac{1}{2} + z$; (ii) $x, y, -1 + z$; (iii) $\frac{3}{2} - x, \frac{1}{2} + y, -\frac{1}{2} + z$.

longest also within the entire range of pressures. Thus, no significant changes in the distribution of protons within the hydrogen bonds surrounding the carboxyl group occur, and consequently the C—O bonds are not affected much (Fig. 6). Interestingly, the long NH···O contact N1—H1A···O2 within a head-to-tail chain in DL-alanine contracts strongly with pressure, so that the N—O distance approaches the value appropriate to qualify the contact as a NH···O hydrogen bond, the value of the N—H—O angle also meeting the geometric criteria (Jeffrey, 1997). Thus, the hydrogen bond linking an NH$_3$ group and a carboxyl group in the chain tends to become three-centered at high pressure (Fig. 5c), similar to what has been observed earlier for other crystalline amino acids (Boldyreva et al., 2005; Minkov, Tumanov et al., 2010; Zakharov et al., 2012).

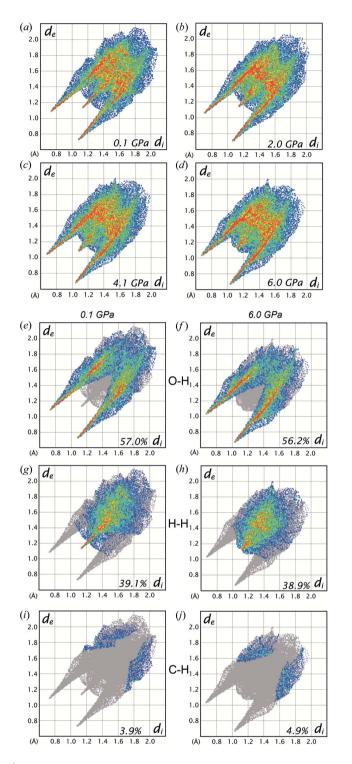**Figure 6**
Pressure-induced changes in the geometry of a carboxyl group and the NH···O hydrogen bonds formed by this group in the crystal structures of L- and DL-alanine.

Figure 7
Void volume versus pressure in L-alanine and DL-alanine. The data for L-alanine are taken from Funnell et al. (2010, 2011) and Tumanov et al. (2010). The data of Funnell et al. are systematically shifted relative to our data, since we used different values of the C—H and N—H distances.
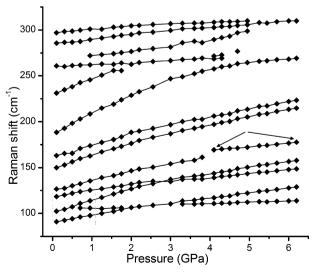
Figure 8
Evolution of two-dimensional Hirshfeld fingerprint plots of DL-alanine structure *versus* pressure [(*a*) 0.1, (*b*) 2.0, (*c*) 4.1 and (*d*) 6.0 GPa]. The color in the sequence white–blue–green–red is a summary of the frequencies of each combination of distances d_e and d_i across the surface of a molecule (in increasing order), where d_i is the internal distance and d_e is the external distance from the Hirshfeld surface to the nearest molecule. (*e*)–(*j*) Decomposed two-dimensional Hirshfeld fingerprint plots of the DL-alanine structure at 0.1 GPa [left column] and 6.0 GPa [right column]. The features along the diagonal are observed because of the H—H contacts (middle row), while the 'wings' are due to O—H contacts (top row). The numbers indicate the percentage of contacts of a certain type.

An important factor driving structural changes in crystalline amino acids at high pressure is reducing the size of voids (Moggach *et al.*, 2008). This factor could be expected to be especially important for alanine since its side chain is not involved in hydrogen-bond formation. The changes in voids with increasing pressure up to ∼ 6 GPa in DL-alanine and, for a comparison, in L-alanine, are shown in Fig. 7. In both structures the main voids are located inside the cyclic motifs formed by six molecules of alanine (Figs. 3 and 4). As the two neighboring molecules are shifted along the *b* axis with increasing pressure, both the total volume of all voids with a selected probe radius 0.2 Å (Fig. 7) and the maximum radius of a void in the structure decrease (the maximum size of voids decreases from 0.79 Å at 0.1 GPa to 0.60 Å at 6.0 GPa in the structure of DL-alanine, and from 0.84 Å at 0.2 GPa to 0.57 Å at 5.9 GPa in the structure of L-alanine).

The analysis of Hirshfeld surfaces and two-dimensional decomposed fingerplots also confirms that, at least up to 6.0 GPa, the compression of alanine crystal structure occurs mostly owing to the decrease in the volume of voids. The contacts between the atoms shorten continuously *versus* pressure, as can be seen in Fig. 8. Reasonably enough, short contacts (corresponding to hydrogen bonds) are compressed to a much lesser extent than the long contacts corresponding to the interactions between the CH_3 groups. The percentage distribution of contacts by type also varies only negligibly (Fig. 9). The largest change observed upon increasing pressure from ambient to 6.0 GPa is the increase in the percentage of C—H contacts by ∼ 1% (from 3.9 to 4.9%) accompanying a decrease in the percentage of O—H contacts (from 57.0 to 56.2%). This phenomenon corresponds to the approaching of CH_3 groups to each other. It should be noted that in the case of L-alanine, the variations in the percentages of contacts were somewhat larger, ∼ 4%, but involved mostly a decrease in the percentage of O—H contacts and an increase in the percen-

Figure 9
Wavenumbers *versus* pressure for the bands in the Raman spectra in the spectral range 70–350 cm^{-1}. Red dashed lines mark the two lowest pressure points at which the spectra have been measured in Belo *et al.* (2010). Arrows indicate the position of the band discussed in text.

tages of contacts belonging to other types (detailed tables presenting the distributions for L-alanine and DL-alanine are given in the supplementary material).

3.2. Raman spectroscopy

The X-ray diffraction study gave no evidence of structural phase transitions within the pressure range studied, either upon slow (days, single-crystal diffraction) or quick (minutes, powder X-ray diffraction using a synchrotron source) pressure variations. Since the conclusion made by Belo *et al.* (2010) on the occurrence of pressure-induced phase transitions in the same system was based on Raman spectroscopy, we also undertook a Raman study of the same samples as studied by X-ray diffraction. The spectra were measured at the pressure varied at a smaller step than in the previous work published by Belo *et al.* (2010). The bands in the spectra were resolved into individual components whenever it was possible and the positions of the band maxima were analyzed. According to our data, no drastic changes occurred in the spectra within the
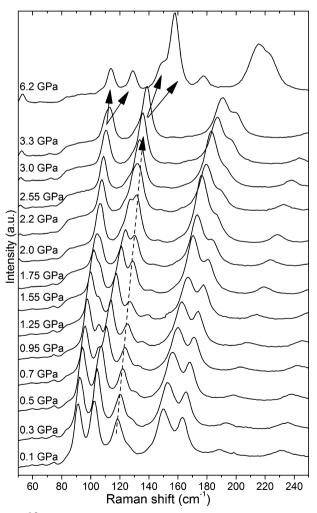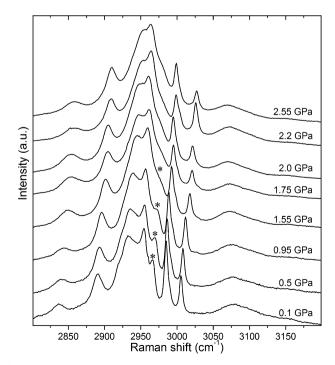
entire pressure range. The apparent appearance or disappearance of any bands was caused by the fact that upon increasing the pressure, different bands in the spectra shifted to a different extent. This was particularly noticeable in the low-wavenumber range (100–300 cm^{-1}) (Fig. 9). The 'interruptions' in the curves plotted in this figure were observed not because of the appearance of new or the disappearance of current bands, but as a result of merging of several bands into one, after which it became impossible to resolve them, or, another way round, as a result of a better bands resolution. With the plot shown at Fig. 9 taken into account, the alterations in the spectra described by Belo *et al.* (2010) can be explained easily without assuming the occurrence of any phase transitions, as we illustrate below.

One of Belo's main arguments in favor of the first phase transition at ∼ 1.7–2.3 GPa was related to 'drastic alterations occurring in the low- and high-wavelength ranges of the spectra at a pressure between 0 and 1.1 GPa' (*i.e.* a significant change in intensity was observed for the bands at 120 cm^{-1}, and a considerable loss in intensity was detected for the band at 2965 cm^{-1}); these phenomena were explained by conformational changes. However, a detailed analysis of our Raman data showed that, in both cases, the changes in intensity were related to different shifts of several existing Raman bands, manifesting itself as the merging of observed bands in the spectra with each other (Figs. 10 and 11). Another indicator of the phase transition given by Belo *et al.* was the disappearance of the band at 140 cm^{-1} at 2.3 GPa. In fact, as can be seen from Fig. 10 (marked with a dashed arrow), this band does not disappear, but the two bands (102 and 118 cm^{-1} in the spec-

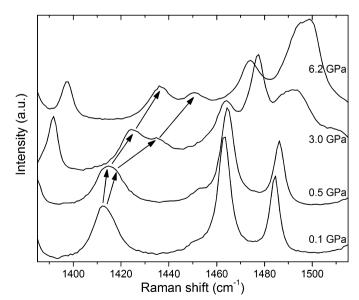**Figure 10**
Raman spectra of DL-alanine at various pressures in the frequency range from 50 to 250 cm^{-1}. The dashed arrow indicates the position of the band at 140 cm^{-1} (ambient pressure). Solid arrows show the separation of the bands merged at 2.2 GPa.

Figure 11
Raman spectra of DL-alanine at various pressures in the frequency range from 2800 to 3200 cm^{-1}. Asterisks mark the position of the band which becomes irresolvable with increasing pressure.

trum measured at the lowest pressure) merge into one at a pressure within 2–4 GPa owing to the difference in the slopes of the pressure dependences (dv/dP) of their maximum positions (Fig. 9). Despite this overlapping, the bands can still be resolved and their positions can be determined. As pressure increased further, the separation of these bands became more evident, especially by 6.2 GPa, the highest pressure point reached in our Raman experiment (Fig. 10, top spectra and solid arrows). Belo *et al.* also associated the phase transition with the changes in intensity of the bands within the range 2850–3100 cm^{-1} observed at 1.7 and 2.3 GPa, but we did not find any significant spectral alterations in this range (Fig. 11), except the aforementioned overlapping of the bands occurring due to the difference in dv/dP.

The next phenomenon described by Belo *et al.* was an increase in the width of the band, which was associated with the torsion vibrations of the CH$_3$ group and the rocking vibrations of the CO$_2$ group (410 and 545 cm^{-1} in the spectrum measured at the lowest pressure, respectively). Indeed, we have also observed a significant increase in the width of the band at 410 cm^{-1}; moreover, the asymmetry of this band became more pronounced upon increasing pressure. Since in the earlier published paper (Fukushima *et al.*, 1959; Machida *et al.*, 1978) this band was associated not only with the torsion vibrations of the CH$_3$ group, but also with the skeletal vibrations, it can be assumed that this band splits into two upon increasing the pressure. Thus, at 6.2 GPa this band can hardly be described as one symmetric peak, but can be fitted very well as two symmetric peaks.[5] The band at 545 cm^{-1} also broadens upon increasing pressure, but much less than that at 410 cm^{-1}, and can be well described as one peak until the highest pressure point. Thus, we cannot relate the observed spectral changes to a disorder of CH$_3$ or CO$_2$ groups, as Belo *et al.* did. The disappearance of the band at 300 cm^{-1} at a pressure between 4.0 and 4.6 GPa, which was considered by Belo *et al.* as evidence of a phase transition, is again associated with the positions of two bands approaching each other (Fig. 9, two upper curves). In our spectra it was possible to resolve these two bands at pressures up to 4.95 GPa, at higher pressure these bands are completely overlapped. Belo *et al.* also described the disappearance of one peak from the group of peaks corresponding to the rocking vibrations of the CH$_3$ group (1017 and 1029 cm^{-1} in the spectrum measured at the lowest pressure) at a pressure between 4.0 and 4.6 GPa. We did not observe this phenomenon; moreover, we managed to resolve the third peak in this group. These three peaks were observed in the spectra measured up to the highest pressure reached in our experiment. The next pressure-induced effect described by Belo *et al.* is a notable change in the intensity of the bands associated with the deformation of CH$_3$ groups and bending of NH$_3$ groups (the spectral range is 1460–1490 cm^{-1}) occurring between 4.0 and 4.6 GPa. However, we managed to resolve not two, but three bands in this group, and their relative intensities changed owing to the overlapping of the

bands. These three bands were observed in our spectra up to the highest pressure reached in the experiment.

Thus, neither our diffraction nor spectral data give any evidence of the occurrence of the first phase transition and conformational changes in DL-alanine in the pressure range below 6.0 GPa. As for the second phase transition reported by Belo *et al.* (in the pressure range from 6.0 to 7.3 GPa), it is difficult for us to comment unambiguously on the spectral changes described by Belo *et al.*, since in our experiments we could measure Raman spectra only at pressures up to 6.2 GPa. Still, based on the Raman measurements at somewhat lower pressures, as well as on the X-ray powder diffraction data, we can try to suggest an alternative interpretation for the effects discussed in Belo's paper. Thus, Belo *et al.* claim the appearance of an extra low-intensity band at 170 cm^{-1} at 6 GPa. We believe that this 'new' band already existed in the spectra measured at lower pressures (Fig. 9, band marked with solid arrows): this band could be observed at 4.1 GPa; below this pressure it is unrecognizable because of its overlapping with the neighboring high-intensity bands. Another argument given by Belo *et al.* (2010) in favor of the second phase transition is the appearance of a band at 1458 cm^{-1} at 7.3 GPa. However, we did resolve this peak also in the spectra measured at pressures from 0.5 GPa up to 6.2 GPa, the highest pressure reached in our Raman experiment (Fig. 12); hence, we call this argument into question. With the data on powder diffraction analysis for this pressure range taken into account, the existence of the second phase transition remains open to question. We are inclined to think that no structural phase transitions occur within this range of pressures either. However, we admit that certain changes in the Raman spectra may be associated with dynamic phase transitions, which we cannot register by X-ray powder diffraction analysis, in particular, with an

Figure 12
Raman spectra of DL-alanine at various pressures in the frequency range from 1380 to 1600 cm^{-1}. Arrows show the changes in the band position with increasing pressure (see text).

---

[5] We could not determine the position of the second peak in all the spectra, since it was difficult to recognize it at low pressures.

research papers

increase in the bifurcated character of NH···O hydrogen bonds within the head-to-tail chains above 6 GPa.

We do not analyze the occurrence of the third phase transition, which was claimed to take place between 11.6 and 13.2 GPa, since we performed no experiments for this range of pressures. However, we would like to note that this is already the pressure range in which the homogeneity of pressure is difficult to achieve, and the crystal structure may be subjected to shear strain, resulting in the formation of defects, disordering and amorphization. In fact, reversible amorphization has been reported recently for L-alanine at 15.46 GPa (Funnell *et al.*, 2011). Taking into account the similarity of the structures of L- and DL-alanine at high pressure, and using Raman data from Belo's work, we can assume an occurrence of reversible amorphization in DL-alanine at pressures of around 15 GPa.

4. Conclusions

Once again, a detailed diffraction study made it possible to 'denounce' the phase transitions, which have been erroneously claimed on the basis of Raman spectroscopy in previous publications. A revision of Raman spectra measured at a better resolution and at a smaller pressure step between the measurements has confirmed that the Raman spectra give no evidence supporting the occurrence of the phase transitions as well: all the pressure-induced changes in the Raman spectra can be explained simply by the fact that the band maxima shift to a different extent under compression. Neither in the structure of DL-alanine nor in the structure of L-alanine could any structural phase transitions be observed at pressures at least up to 8.3 GPa. The *b* and *c* cell parameters become accidentally equal at some pressure point (1.5–2.0 GPa), owing to the anisotropic lattice strain, but then diverge again, while the space-group symmetry does not change. In contrast to what has been observed for chiral and racemic counterparts of serine and cysteine, the structural response of L- and DL-alanine to increasing pressure is very similar and is related mainly to the closing of voids. The anisotropy of strain correlates with the directions of hydrogen-bonded motifs. The NH···O hydrogen bonds within the head-to-tail chains in DL-alanine tend to become bifurcated at pressures above 6 GPa. For L-alanine the effect is similar.

References

Ahsbahs, H. (1996). *Z. Kristallogr.* Suppl. **11**, 30.
Ahsbahs, H. (2004). *Z. Kristallogr.* **219**, 305–308.
Allen, F. H., Johnson, O., Shields, G. P., Smith, B. R. & Towler, M. (2004). *J. Appl. Cryst.* **37**, 335–338.
Angel, R. J. (2004). *J. Appl. Cryst.* **37**, 486–492.
Belo, E. A., Lima, J. A. Jr, Freire, P. T. C., Melo, F. E. A., Filho, J. M., Bordallo, H. N. & Polian, A. (2010). *Vib. Spectrosc.* **54**, 107–111.
Boehler, R. (2006). *Rev. Sci. Instrum.* **77**, 115103.
Boldyreva, E. V. (2007). *Cryst. Growth Des.* **7**, 1662–1668.
Boldyreva, E. V. (2008*a*). *Models, Mysteries & Magic of Molecules*, edited by J. C. A. Boeyens & J. F. Ogilvie, pp. 167–192. Dordrecht: Springer.
Boldyreva, E. V. (2008*b*). *Acta Cryst.* A**64**, 218–231.
Boldyreva, E. V. (2009). *Phase Transitions*, **82**, 303–321.
Boldyreva, E. V., Ivashevskaya, S. N. & Sowa, H. (2005). *Z. Kristallogr.* **220**, 50–57.
Boldyreva, E. V., Kolesnik, E. N. & Drebushchak, T. N. (2006). *Z. Kristallogr.* **221**, 150–161.
Boldyreva, E. V., Sowa, H., Seryotkin, Y. V., Drebushchak, T. N., Ahsbahs, H., Chernyshev, V. V. & Dmitriev, V. (2006). *Chem. Phys. Lett.* **429**, 474–478.
Boultif, A. & Louër, D. (2004). *J. Appl. Cryst.* **37**, 724–731.
Brock, C. P., Schweizer, W. B. & Dunitz, J. D. (1991). *J. Am. Chem. Soc.* **113**, 9811–9820.
Budzianowski, A. & Katrusiak, A. (2004). *High-Pressure Crystallography*, edited by A. Katrusiak & P. F. McMillan, pp. 101–112. Dordrecht: Kluwer Academic Publishers.
Destro, R., Soave, R. & Barzaghi, M. (2008). *J. Phys. Chem. B*, **112**, 5163–5174.
Drebushchak, T. N., Sowa, H., Seryotkin, Y. V., Boldyreva, E. V. & Ahsbahs, H. (2006). *Acta Cryst.* E**62**, o4052–o4054.
Forman, R. A., Piermarini, G. J., Barnett, J. D. & Block, S. (1972). *Science*, **176**, 284–285.
Freire, P. T. C. (2010). *High-Pressure Crystallography*, edited by E. Boldyreva & P. Dera, pp. 559–572. Dordrecht: Springer.
Fukushima, K., Onishi, T. & Shimanouchi, T. (1959). *Spectrochim. Acta*, **15**, 236–241.
Funnell, N. P., Dawson, A., Francis, D., Lennie, A. R., Marshall, W. G., Moggach, S. A., Warren, J. E. & Parsons, S. (2010). *CrystEngComm*, **12**, 2573–2583.
Funnell, N. P., Marshall, W. G. & Parsons, S. (2011). *CrystEngComm*, **13**, 5841–5848.
Görbitz, C. H. (1989). *Acta Cryst.* B**45**, 390–395.
Hammersley, A. P., Svensson, S. O., Hanfland, M., Fitch, A. N. & Hausermann, D. (1996). *High Pressure Res.* **14**, 235–248.
Jeffrey, G. A. (1997). *An Introduction to Hydrogen Bonding*. New York: Oxford University Press.
Kolesnik, E. N., Goryainov, S. V. & Boldyreva, E. V. (2005). *Dokl. Phys. Chem.* **404**, 169–172.
Machida, K., Kagayama, A. & Saito, Y. (1978). *J. Raman Spectrosc.* **7**, 188–193.
Macrae, C. F., Bruno, I. J., Chisholm, J. A., Edgington, P. R., McCabe, P., Pidcock, E., Rodriguez-Monge, L., Taylor, R., van de Streek, J. & Wood, P. A. (2008). *J. Appl. Cryst.* **41**, 466–470.
McKinnon, J. J., Jayatilaka, D. & Spackman, M. A. (2007). *Chem. Commun.* pp. 3814–3816.
McKinnon, J. J., Spackman, M. A. & Mitchell, A. S. (2004). *Acta Cryst.* B**60**, 627–668.
Minkov, V. S., Goryainov, S. V., Boldyreva, E. V. & Görbitz, C. H. (2010). *J. Raman Spectrosc.* **41**, 1748–1758.
Minkov, V. S., Krylov, A. S., Boldyreva, E. V., Goryainov, S. V., Bizyaev, S. N. & Vtyurin, A. N. (2008). *J. Phys. Chem. B*, **112**, 8851–8854.
Minkov, V. S., Tumanov, N. A., Kolesov, B. A., Boldyreva, E. V. & Bizyaev, S. N. (2009). *J. Phys. Chem. B*, **113**, 5262–5272.

Minkov, V. S., Tumanov, N. A., Quesada Cabrera, R. & Boldyreva, E. V. (2010). *CrystEngComm*, **12**, 2551–2560.

Moggach, S. A., Allan, D. R., Clark, S. J., Gutmann, M. J., Parsons, S., Pulham, C. R. & Sawyer, L. (2006). *Acta Cryst.* B**62**, 296–309.

Moggach, S. A., Allan, D. R., Morrison, C. A., Parsons, S. & Sawyer, L. (2005). *Acta Cryst.* B**61**, 58–68.

Moggach, S. A., Marshall, W. G. & Parsons, S. (2006). *Acta Cryst.* B**62**, 815–825.

Moggach, S. A., Parsons, S. & Wood, P. A. (2008). *Crystallogr. Rev*. **14**, 143–184.

Oxford Diffraction (2010). *CrysAlis Pro*. Oxford Diffraction Ltd, Abingdon, England.

Piermarini, G. J. (1973). *J. Appl. Phys.* **44**, 5377–5382.

Piermarini, G. J., Block, S., Barnett, J. D. & Forman, R. A. (1975). *J. Appl. Phys.* **46**, 2774–2780.

Sheldrick, G. M. (2008). *Acta Cryst.* A**64**, 112–122.

Simpson, H. J. & Marsh, R. E. (1966). *Acta Cryst.* **20**, 550–555.

Sowa, H. & Ahsbahs, H. (2006). *J. Appl. Cryst.* **39**, 169–175.

Spek, A. L. (2009). *Acta Cryst.* D**65**, 148–155.

Staun Olsen, J., Gerward, L., Freire, P. T. C., Mendes Filho, J., Melo, F. E. A. & Souza Filho, A. G. (2008). *J. Phys. Chem. Solids*, **69**, 1641–1645.

Staun Olsen, J., Gerward, L., Souza Filho, A. G., Freire, P. T. C., Mendes Filho, J. & Melo, F. E. A. (2006). *High Pressure Res.* **26**, 433–437.

Stoe & Cie (2002). *X-Step*. Stoe & Cie GmbH, Darmstadt, Germany.

Stoe & Cie (2007). *WinXPOW*. Stoe & Cie GmbH, Darmstadt, Germany.

Teixeira, A. M. R., Freire, P. T. C., Moreno, A. J. D., Sasaki, J. M., Ayala, A. P., Mendes Filho, J. & Melo, F. E. A. (2000). *Solid State Commun.* **116**, 405–409.

Tumanov, N. A., Boldyreva, E. V., Kolesov, B. A., Kurnosov, A. V. & Quesada Cabrera, R. (2010). *Acta Cryst.* B**66**, 458–471.

Vinogradov, S. N. (1979). *Int. J. Pept. Protein Res.* **14**, 281–289.

Wallach, O. (1895). *Justus Liebigs Ann. Chem.* **286**, 90–118.

Wolff, S. K., Grimwood, D. J., McKinnon, J. J., Jayatilaka, D. & Spackman, M. A. (2007). *CrystalExplorer*, Version 2.1, Technical Report. University of Western Australia, http://hirshfeldsurface.net/.

Zakharov, B. A., Kolesov, B. A. & Boldyreva, E. V. (2012). *Acta Cryst.* B**68**, 275–286.